Unexpected Binding Mode for 2′-Phosphoadenosine-Based Nucleotide Inhibitors in Complex with Human Angiogenin Revealed by Heteronuclear NMR Spectroscopy†

Kenji Tonan,‡,§ Ping Xu,‡ Jeremy L. Jenkins,|| Aniello Russo,||,⊥ Robert Shapiro,||,# and Feng Ni*,‡,§

Biomolecular NMR and Protein Research Group, Biotechnology Research Institute, National Research Council of Canada, 6100 Royalmount Avenue, Montreal, Quebec, H4P2R2, Canada, Department of Biochemistry, McGill University, Montreal, Quebec, Canada, and the Center for Biochemical and Biophysical Sciences and Medicine and Department of Pathology, Harvard Medical School, Cambridge, Massachusetts 02139

Received March 14, 2003; Revised Manuscript Received April 24, 2003

ABSTRACT: Human angiogenin (Ang) is a tumor-promoting RNase in the pancreatic RNase superfamily. Efforts to develop nucleotide-based inhibitors of Ang as potential anticancer drugs have been hampered by the lack of direct structural information on Ang−nucleotide complexes. Here, we have used heteronuclear NMR spectroscopy with ^{15}N- and $^{15}N/^{13}C$-labeled Ang to map the interactions of Ang with the phosphate ion, seven adenosine mononucleotides (the 2′-, 3′-, and 5′-monophosphates, the 2′,5′- and 3′,5′-diphosphates, the 5′-diphosphate, and the 2′-monophospho-5′-diphosphate), and the dinucleotide 2′-deoxyuridine 3′-pyrophosphate (P′ → 5′) adenosine-2′-phosphate (dUppA-2′-p). The 2′-phosphate based derivatives, which bind more tightly than the corresponding 3′-phosphate isomers, induced characteristic large resonance perturbations of the backbone amide proton of Leu^{115}, the backbone ^{15}N of His^{114}, and the Gln^{12} side-chain NH_2 group in the Ang active site. In contrast, adenosine derivatives with only 3′- or 5′-phosphates produced much less dramatic perturbations of Leu^{115} and His^{114} resonances, along with modest perturbations of additional residues both within and beyond the active site. Measurements of NOEs together with molecular docking analyses revealed the three-dimensional structures of the complexes of Ang with adenosine 2′,5′-diphosphate and dUppA-2′-p; the binding modes of these inhibitors differ substantially from those predicted in earlier studies. Most notably, the 2′-phosphate rather than the 5′-phosphate occupies the P_1 catalytic subsite of Ang, and the side chain of His^{114} has undergone a conformational transition that positions it outside P_1 and allows it to form stacking interactions with the adenine ring of the inhibitor. Strikingly, the 2′-deoxyuridine moiety of dUppA-2′-p makes only a few contacts with Ang, and these involve residues outside the B_1 subsite where the pyrimidine ring of substrates normally binds.

Human angiogenin (Ang),[1] a monomeric protein of 123 amino acids, is a unique member of the pancreatic RNase superfamily that induces angiogenesis in vivo (*1*, *2*) and has been implicated as an important factor contributing to the development of human tumors (*3*−*7*). Ang exhibits a characteristic ribonucleolytic activity that is several orders of magnitude weaker than that of RNase A (*8*, *9*) but nonetheless essential for its angiogenic and tumor-promoting activities (*10*−*12*). There is, therefore, significant interest in the design and discovery of small molecule inhibitors of the enzymatic activity of Ang as antitumor agents (*13*−*15*).

Ang and other RNases of the same superfamily all cleave $P-O^{5'}$ bonds of RNA specifically after pyrimidine residues to leave a 2′,3′-cyclic phosphate group, and all prefer purine nucleotides on the opposite side of the scissile bond (reviewed in refs *16*−*19*). Several three-dimensional structures of human Ang have been determined, including three crystal structures of the free enzyme (*20*, *21*), two crystal structures of complexes with small inorganic molecules (phosphate and pyrophosphate ions) (*22*), and one solution structure by use of NMR spectroscopy (*23*). These structures show that the architecture of the P_1 subsite where phosphodiester bond cleavage occurs corresponds closely to that in RNase A; this site includes the catalytic triad $His^{13}/Lys^{40}/His^{114}$ ($His^{12}/Lys^{41}/His^{119}$ in RNase A), as well as the side chain of Gln^{12} and main-chain NH of Leu^{115} (Gln^{11} and Phe^{120}, respectively, in RNase A) (*21*, *22*, *24*, *25*). However, the key pyrimidine-binding subsite, B_1, is obstructed by the C-terminal segment of Ang, which travels in a markedly

† This work was supported by the National Institutes of Health, U.S.A. (Grant CA88738 to R.S. and subcontracted to McGill University) and the National Research Council of Canada (NRCC Publication 46155).

* Corresponding author. Phone: (514) 496-6729. Fax: (514) 496-5143. E-mail: Feng.Ni@cnrc-nrc.gc.ca.

‡ National Research Council of Canada.

§ McGill University.

|| Center for Biochemical and Biophysical Sciences and Medicine, Harvard Medical School.

⊥ Present address: Department of Life Sciences, Second University of Naples, Via Vivaldi 43, Caserta, Italy.

Department of Pathology, Harvard Medical School.

[1] Abbreviations: Ang, angiogenin; RNase A, bovine pancreatic ribonuclease A; HSQC, heteronuclear single quantum coherence; P_i, phosphate ion; A, adenosine; A-2′-p, adenosine 2′-phosphate; pA-2′-p, adenosine 2′,5′-diphosphate; ppA-2′-p, 5′-diphosphoadenosine 2′-phosphate; dUppA-2′-p, 2′-deoxyuridine 3′-pyrophosphate (P′ → 5′) adenosine-2′-phosphate; pA, adenosine 5′-phosphate; ppA, adenosine 5′-diphosphate; A-3′-p, adenosine 3′-phosphate; pA-3′-p, adenosine 3′,5′-diphosphate; pdUppA-3′−p, 5′-phospho-2′-deoxyuridine 3′-pyrophosphate (P′ → 5′) adenosine 3′-phosphate; EDN, eosinophil-derived neurotoxin; ECP, eosinophil cationic protein.

10.1021/bi030066h CCC: $25.00
Published on Web 09/06/2003

different direction from that in RNase A and contains a four-residue extension. This blockage is achieved primarily by the positioning of residue Gln^{117} (corresponding to residue Ala^{122} in RNase A) within B_1 and is one of several structural features responsible for the low enzymatic activity of Ang (see refs *22* and *26*). Another is the inadequate structuring of the B_2 purine-binding subsite, which is much more open than that in RNase A and lacks analogues for three B_2 components of that enzyme (Asn^{71}, Gln^{69}, and Asn^{67}).

Attempts to develop nucleotide inhibitors of Ang have not been as successful as parallel efforts with RNase A (*14*, *27*, *28*). For RNase A, investigation of a series of adenosine nucleotides showed that tight binding could be achieved by incorporating a 5′-pyrophosphate and a 2′- or 3′-monophosphate group, with a further advantage conferred by attaching a pyrimidine nucleotide to the pyrophosphate through its 3′-oxygen. K_i values for the most avid of these inhibitors were in the range of 10^{-8} to 10^{-7} M. Application of this same strategy with Ang (*13*) yielded inhibitors whose affinities were considerably higher than those of simple substrates and nucleoside monophosphates but still orders of magnitude weaker than had been measured with RNase A. The best of these nucleotide inhibitors are 5′-diphosphoadenosine 2′-phosphate (ppA-2′-p) and its 2′-deoxyuridine derivative dUppA-2′-p and NADPH, all with K_i values of $\sim 10^{-4}$ M with Ang (*13*, *14*, *29*).

Information on the three-dimensional structures of Ang−nucleotide complexes should be helpful for the development of more potent inhibitors to target the unique substrate binding sites of Ang. Although nucleotide complexes of other members of the RNase superfamily have been extensively investigated by X-ray crystallography and NMR, no structural studies on Ang−nucleotide complexes have been reported to date. Crystallographic efforts in particular have been impeded because residues from neighboring Ang molecules impinge upon the B_2 region of the active site in all available Ang crystal forms (*22*). Therefore, attempts to understand the potency and selectivity of Ang inhibitors have been based on models constructed by analogy with known RNase A complex structures (*13*, *30*). In these models, inhibitors such as ppA-2′-p and its 3′-phosphate isomers were assumed to adopt the same general binding mode as substrates, with the pyrophosphate in P_1 and the 2′- or 3′-phosphate group in the P_2 subsite. The preference of Ang for a 2′- versus a 3′-phosphate (contrasting with the preference of RNase A for a 3′-phosphate) was then interpreted in terms of the positioning of the P_2 site residue Arg^5 (which differs from that of the P_2 residues Lys^7 and Arg^{10} in RNase A). Binding of the dinucleotide dUppA-2′-p was thought to require a substantial structural reorganization to allow access of the pyrimidine ring to the B_1 site, as has been postulated to occur during the normal catalytic pathway for substrate cleavage.

Here, we have examined the interactions of Ang with a series of related nucleotide inhibitors, using binding-induced resonance perturbations of ^{15}N- and $^{15}N/^{13}C$-labeled Ang. Specifically, we have measured the $^{15}N,^{1}H$-HSQC spectra of ^{15}N-labeled Ang in the presence of phosphate ion (P_i), adenosine (A), and the adenosine-based nucleotides A-2′-p (adenosine 2′-phosphate), pA-2′-p (adenosine 2′,5′-diphosphate), ppA-2′-p, pA (adenosine 5′-phosphate), ppA (adenosine 5′-diphosphate), A-3′-p (adenosine 3′-phosphate),

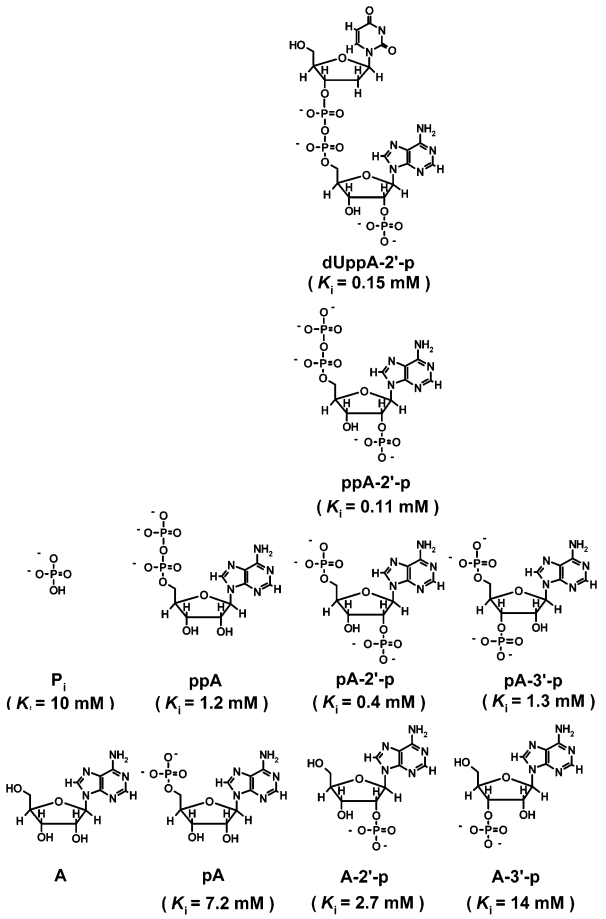

FIGURE 1: Structures and abbreviations of inhibitors used for the present study. K_i values determined kinetically at pH 5.9 in 0.2 M MES-NaOH (*13*, *22*) are shown in parentheses.

pA-3′-p (adenosine 3′,5′-diphosphate), and dUppA-2′-p, for which K_i values with Ang have been determined previously (ref *13*; Figure 1). Extensive resonance perturbations of the P_1 and/or B_2-subsite residues of Ang were induced by the phosphate and all nucleotide compounds, indicating the validity of this approach. Interestingly, we found that 2′-phosphoadenosine-based inhibitors appear to interact with Ang more specifically than the 3′- and 5′-phosphoadenosine derivatives. More significantly, NOE measurements with both free and inhibitor-bound Ang were used to derive three-dimensional structures for Ang in complex with the 2′-phosphoadenosine-based nucleotides pA-2′-p and dUppA-2′-p. Both inhibitors were found to adopt binding modes that differ strikingly from those anticipated.

MATERIALS AND METHODS

Reagents and Inhibitors. All chemicals were analytical grade and purchased from commercial sources. Sodium phosphate was from BDH (Toronto, Canada). Adenosine nucleotides were from Sigma-Aldrich except for ppA-2′-p and dUppA-2′-p, which were synthesized by a combined chemical and enzymatic procedure as described previously (*13*, *30*).

Preparations of ^{15}N- and $^{15}N/^{13}C$-labeled Ang. A synthetic gene for Met^{-1} Ang (*31*) with its *Nde1* and *BamH1* sites removed by site-directed mutagenesis (*32*) was inserted into the unique *Nde1* and *BamH1* sites of the vector pET11a (*33*) and transformed into *Escherichia coli* (*34*). Cells were grown

in M9 medium (*35*) containing ^{15}N-ammonium sulfate with 99% ^{15}N enrichment (Isotech) as the sole nitrogen source and supplemented with 1 mM $MgSO_4$, 0.1 mM $CaCl_2$, 5 μg/mL $FeCl_3$, 1 μg/mL thiamine, 50 μg/mL ampicillin, and 1% D-glucose (either unlabeled or labeled with ^{13}C at 99% enrichment (Isotech)) as the sole significant carbon source. A 1 mL volume of starter cultures (one for each 2 L of final culture) was inoculated with 5 μL of cryopreserved culture and grown at 37 °C with shaking (300 rpm) until slightly turbid (6−8 h). Each of these cultures was added to 100 mL of medium and grown in the same manner for 12−14 h. Cells were then harvested by centrifugation, resuspended in 6 mL of medium per 100 mL of culture, and 3 mL was added to 1 L of medium. These cultures were grown to an A_{600} of 0.6−0.9, at which time IPTG (isopropyl β-thiogalactoside) was added to a final concentration of 1 mM. Cells were harvested after another 3 h of growth. Ang was obtained in high yield (∼15 mg/L) by the purification procedure for mouse angiogenins described by Holloway et al. (*36*).

NMR Sample Preparation. ^{15}N-labeled Ang for ^{15}N,^{1}H-HSQC measurements was prepared at a concentration of 0.1−0.15 mM in a buffer containing 50 mM sodium acetate, 0.2 mM EDTA, and 5−10% (v/v) $^{2}H_2O$ at pH 5.0. For titration experiments with the phosphate ion and nucleotide inhibitors, a stock solution of each inhibitor (7.5−90 mM) was prepared in the acetate buffer, with the pH adjusted to 5.0. For NOE and ^{13}C,^{1}H-HSQC measurements, samples of ^{15}N/^{13}C-labeled Ang were prepared in the nucleotide-free state and in the presence of a 10−15-fold molar excess of pA-2′-p or a 6.3-fold molar excess of dUppA-2′-p at protein concentrations of 0.9−1.0 mM and in the same buffer solution except for the use of deuterated sodium acetate-d_3. The higher protein concentrations and sodium acetate-d_3 used did not cause any differences in the protein NMR spectra, as verified by using ^{15}N-labeled Ang samples at concentrations ranging from 0.1 to 1.2 mM.

NMR Experiments. Two-dimensional ^{15}N,^{1}H-HSQC spectra were recorded at 298 K using Bruker 500 MHz NMR spectrometers (DRX-500 or Avance-500). The proton carrier frequency was placed on the water resonance, and the solvent signal was suppressed by a WATERGATE pulse sequence (*37*). The ^{15}N,^{1}H-HSQC spectra were acquired with 1024 (t_2) × 128 (t_1) data points and processed using the NMRPipe/NMRDraw software program (*38*). The spectral resolutions after processing were 6.0 and 10.9 Hz along the F_2 (H^N) and F_1 (^{15}N) dimensions, respectively. Three-dimensional NMR spectra for the ^{15}N/^{13}C-labeled Ang samples, including double- and triple-resonance experiments HNCACB, CBCA(CO)NH, HBHA(CO)NH (*39*), HCCH-TOCSY (*40*), NOESY-^{15}N,^{1}H-HSQC (*41*), and NOESY-aromatic ^{13}C,^{1}H-HSQC, were recorded at 298 K on an 800 MHz spectrometer (Bruker: Avance-800). The mixing times were 21.0 ms for HCCH-TOCSY and 120.0 ms for 3-D NOESY experiments, respectively. In all the experiments, ^{15}N-decoupling during the detection period was achieved by applying a 1.0 kHz GARP sequence (*42*). Three experiments, HCCH-TOCSY, NOESY-^{15}N,^{1}H-HSQC, and NOESY-aromatic ^{13}C,^{1}H-HSQC, were modified to remove the extra heteronuclear couplings caused by the additional isotope. In HCCH-TOCSY and NOESY-aromatic ^{13}C,^{1}H-HSQC experiments, ^{15}N couplings were removed by applying a 1.0 kHz GARP sequence throughout the t_1 and t_2 time periods. In NOESY-^{15}N,^{1}H-HSQC, ^{13}C splittings were refocused by using ^{13}C refocusing pulses at 42.0 ppm in the t_1 and t_2 periods and by applying a 1.5 kHz ^{13}C SEDUCE-1 (*43*) at 125.0 ppm in the ^{1}H evolution period and at 176.0 ppm in the ^{15}N evolution period. Aromatic side-chain proton assignments were achieved by performing the (HB)CB(CGCD)HD and (HB)CB(CGCDCE)HE experiments (*39*). In ^{13}C,^{1}H-HSQC experiments, a 1.0 kHz GARP was applied to the ^{15}N nuclei during the evolution period.

Three different experimental schemes were used with the 800 MHz spectrometer to collect intraligand (transferred) and intermolecular NOEs originating from the nucleotide protons. For the Ang-[dUppA-2′-p] complex, all nucleotide and Ang protons were allowed to evolve during the t_1 time period, and only the nucleotide proton signals were detected during acquisition. All cross-peaks, including intraligand and intermolecular NOEs, had the same sign as the diagonal signals, indicating that these NOEs are from the Ang−nucleotide complex but transferred to the free nucleotide (transferred NOEs). Intermolecular NOEs appeared asymmetrically in the spectrum while intranucleotide transferred NOEs were found in symmetry-related locations. Intermolecular NOEs were also identified by comparing the NOESY spectra acquired with and without simultaneous ^{15}N/^{13}C decoupling during t_1. For the Ang-[pA-2′-p] complex, the intraligand and intermolecular NOEs were observed in a NOESY experiment whereby Ang proton resonances were suppressed during the t_1 evolution followed by the detection of all nucleotide and Ang proton signals during t_2. For both complexes, intermolecular NOEs were also observed selectively by frequency-labeling of the ^{13}C magnetization of Ang during t_1, which was transferred to the ^{13}C-attached protons before the NOE mixing period and followed by detection of nucleotide protons during t_2. The intermolecular NOESY experiments were carried out using a previously published procedure (*44*) modified to incorporate a WATERGATE sequence (*37*) and selective detection of nucleotide protons during t_2.

Structure Calculations Using NMR and NOE-Derived Constraints. Structure calculations using NOE-derived distance restraints were carried out by a simulated annealing procedure implemented in the CNS version 1.0 program interfaced with ARIA (*45*, *46*). A total of 4360 NOE peaks were identified for free Ang from the 3-D NOESY spectra: 1024 from NOESY-^{15}N,^{1}H-HSQC, 175 from NOESY-aromatic ^{13}C,^{1}H-HSQC, and 3161 from NOESY-^{13}C,^{1}H-HSQC. For the dUppA-2′-p complex, a total of 3933 NOE peaks were identified, including 1096 from NOESY-^{15}N,^{1}H-HSQC, 226 from NOESY-aromatic ^{13}C,^{1}H-HSQC, and 2611 from NOESY-^{13}C,^{1}H-HSQC. Lists of the NOE peaks were iteratively assigned as unique and ambiguous NOE distance restraints using a procedure described previously (*47*). The X-ray structure of Ang (*20*) was employed to calculate an initial contact map and a loosely folded starting structure of Ang, by adding a deviation of 8 Å to all the atomic coordinates. This starting structure template was used to filter spectral artifacts and reduce the number of ambiguous NOE distance constraints to manageable levels (*45*, *46*). Dihedral angles based on the ^{13}C chemical shift index (*48*) were also included as additional constraints in the refinement stage of the structure calculations. Thirty-four residues with ^{13}C shift differences, [$^{13}C^{\alpha} - {}^{13}C^{\beta}$], deviating by more than 2 ppm

from the random-coil values (deposited in www.bmrb.wisc.edu) (*48*), were used to constrain the backbone dihedral angles to the α-helical conformations, $-85° < \phi < -45°$ and $-55° < \psi < -15°$. The backbone conformations of 47 residues, of which [$^{13}C^{\alpha} - {}^{13}C^{\beta}$] deviated −2 ppm or less from the random-coil values, were constrained to β-strand conformations with $-155° < \phi < -115°$ and $+115° < \psi < +155°$. The degree of assignment ambiguity and the tolerance of violated distance constraints (*45*) were adjusted in iterative steps to arrive at the structure solutions with converged NOE assignment lists. The contact maps through the iterations were convergent together with the improvements of the calculated structure models.

Calculation of Dissociation Constants, K_D, Using Binding-Induced Resonance Perturbations. Binding-induced chemical shift changes in the $^{15}N,^{1}H$-HSQC spectra of Ang were measured for the phosphate ion (up to 360 mol excess) and adenosine nucleotide inhibitors, A (up to 420 mol excess), A-3′-p (up to 210 mol excess), pA (up to 210 mol excess), A-2′-p (up to 105 mol excess), pA-3′-p (up to 60 mol excess), ppA (up to 60 mol excess), pA-2′-p (up to 21 mol excess), and ppA-2′-p (up to 6.1 mol excess). Dissociation constants, K_D, of each nucleotide inhibitor were calculated from the dependence of the observed resonance perturbations of various Ang residues on inhibitor concentration using the equation

$$\Delta\nu/\Delta\nu_{max} = [I]/(K_D + [I])$$

where $\Delta\nu$ and $\Delta\nu_{max}$ are the resonance perturbations at inhibitor concentration [I] and at saturation, respectively. The total inhibitor concentrations were used for values of [I] because depletion by Ang is minimal when $[I]_{total} \gg [Ang]$. Four to eight increments of inhibitor concentrations were used to obtain titration data for evaluating the K_D values.

Docking Analysis of Ang−Nucleotide Complexes. Flexible ligand docking of pA-2′-p to Ang was performed with AutoDock 3.0.5 employing a Lamarckian Genetic Algorithm (LGA) (*49*). The LGA performs flexible docking by combining a genetic algorithm with an adaptive local search method to minimize interaction energy. Docking configurations are evaluated based on an empirical energy scoring function that has been calibrated to 30 protein−ligand complexes with known structures and binding constants. The coordinates for pA-2′-p with C2′*endo*/C3′*exo* and C3′*endo* ribose puckering were taken from the crystal structures of the EDN-[pA-2′-p] (*50*) and RNase A-[ppA-2′-p] complexes (*51*), respectively. Ang coordinates were taken from the 1.8 Å resolution crystal structure of free Ang (ref *21*; PDB code 1B1I). Protonation states were assigned in Insight II (Accelrys), and atom potentials and partial charges were assigned with the CFF91 force field. A 26.25 $Å^3$ docking grid, centered at the position occupied by the phosphorus atom in the Ang−phosphate complex (ref *22*; PDB code 1HBY), was created with the AutoGrid program. Default LGA parameters were used, except that ligands were initially positioned at the grid center, and 10 docking runs with 1.5×10^6 energy evaluations each were carried out. An initial model of Ang complexed with dUppA-2′-p was generated in Insight II by fusing dUp [taken from the X-ray coordinates of the complex of RNase A with 5′-phospho-2′-deoxyuridine 3′-pyrophosphate (P′ → 5′) adenosine 3′-phosphate (pdUppA-3′-p) (PDB code 1QHC)] onto an AutoDock model for pA-2′-p. Manual adjustments to the dUp portion of this structure were performed, and the models obtained were energy minimized in Discover (Accelrys) using the CFF91 force field and conjugate gradients minimization (100 steps), with the A-2′-p position held fixed.

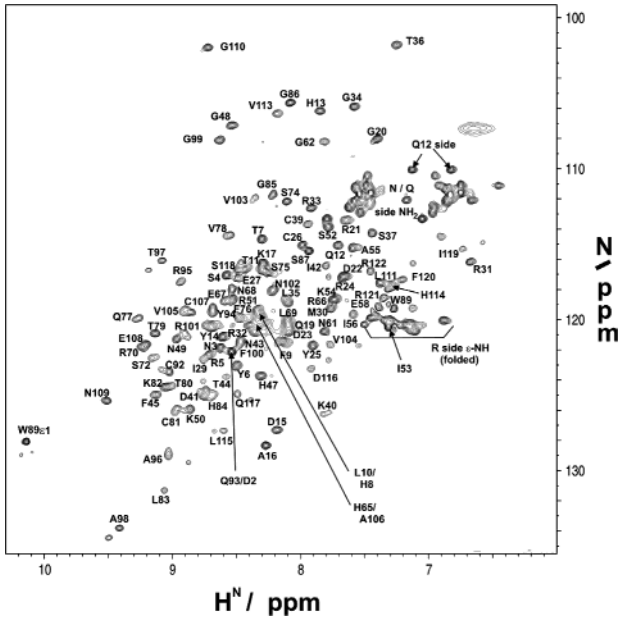

FIGURE 2: 500 MHz $^{15}N,^{1}H$-HSQC spectrum of ^{15}N-labeled Ang at a concentration of 0.15 mM in a buffer of 50 mM sodium acetate containing 0.2 mM EDTA, at pH 5.0 and 298 K.

RESULTS

Resonance Assignments and Assessment of the Three-Dimensional Structure of Free Ang in Solution. Studies on free Ang were performed at pH 5.0 in 50 mM sodium acetate; this buffer does not influence the enzymatic activity of Ang (Russo, A. and Shapiro, R., unpublished experiments), and we therefore presume that neither Na^+ nor acetate ion binds to the active site region. Residue-specific assignments of the ^{1}H and ^{15}N resonances of the backbone and side-chain amide groups were achieved through sequential and intraresidue connectivities in the HNCACB and CBCA(CO)NH spectra of $^{15}N/^{13}C$-labeled Ang. Figure 2 shows an $^{15}N,^{1}H$-HSQC spectrum of the ^{15}N-labeled (or $^{15}N/^{13}C$-labeled) protein. Of all the backbone amide groups, those for Gln^{1}, Lys^{60}, and Lys^{73} were not identified, and signals for some residues (His^{8}, Thr^{11}, Gln^{19}, Ile^{53}, Asn^{59}, His^{65}, Arg^{66}, Ile^{71}, Ala^{106}, and Ser^{118}) overlapped with others. Most of the side-chain NH_2 groups of Asn and Gln were assigned to specific residues. A weaker $^{15}N,^{1}H$-HSQC signal was observed for each amide group of residues Lys^{40}, Cys^{92}, Ala^{96}, Thr^{97}, Ala^{98}, and Leu^{115} and the indole ε-NH Trp^{89} as reported previously for Ang in a phosphate buffer (*23*).

Assignments of the observed $^{13}C^{\alpha}$ and $^{13}C^{\beta}$ resonances in the HNCACB and CBCA(CO)NH spectra allowed an assessment of the secondary structure of free Ang in solution based on the ^{13}C chemical shift index (*48*). No differences were found at the secondary structure level for free Ang in solution and in the crystalline state (data not shown). In addition, a low-resolution structure calculated using NOE distance constraints from the 3-D NOESY-$^{15}N,^{1}H$-HSQC and NOESY-$^{13}C,^{1}H$-HSQC measurements and dihedral angle

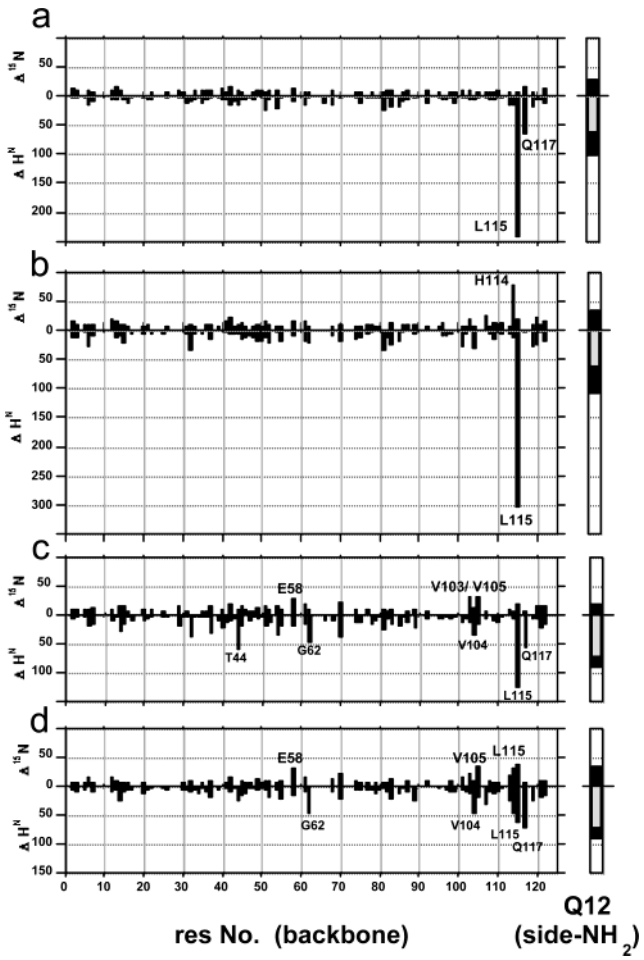

FIGURE 3: Perturbations (in Hz or $500.13 \times |\Delta\delta_H|$ for proton and $50.68 \times |\Delta\delta_H|$ for ^{15}N) of the ^1H and ^{15}N resonances of the backbone amide groups and the side-chain NH_2 group of Gln^{12} of ^{15}N-labeled Ang by (a) P_i (at 360 mol excess), (b) A-2′-p (at 105 mol excess), (c) A-3′-p (at 210 mol excess), and (d) pA (at 210 mol excess) measured in a buffer of 50 mM sodium acetate containing 0.2 mM EDTA, at pH 5.0 and 298 K. The concentrations of Ang were in the range of 0.1−0.14 mM. The different parts in the bars of the Gln^{12} side chain depict each of the perturbations of the syn (hatched) and anti (black) amine protons of the NH_2 group.

constraints based on the ^{13}C chemical shift index reproduced essentially the same secondary and tertiary folds of the Ang backbone as those of free Ang in the crystaline state (*20*−*22*). Therefore, there do not appear to be major structural differences between free Ang in solution and in the crystal, in agreement with previous findings (*23*).

^1H and ^{15}N Resonance Perturbations of Ang Residues Induced by P_i and Adenosine Monophosphates. The binding of inhibitors to Ang was characterized by measuring the ^{15}N,^1H-HSQC spectra of ^{15}N-labeled Ang in the presence of varying amounts of these molecules. Figure 3 shows the resonance perturbations about the backbone amide and the Gln^{12} side-chain NH_2 groups by saturating amounts of P_i and the three kinds of adenosine monophosphate derivatives, A-2′-p, A-3′-p, and pA. Adenosine itself did not cause appreciable changes for any residues even at concentrations as high as 35 mM (data not shown). A large excess of P_i induced dramatic and differential resonance perturbations of the backbone amide protons of Leu^{115} and Gln^{117} and the Gln^{12} side-chain NH_2 group (Figure 3a) (effects on side-chain NH groups of other residues—e.g., His^{13}, Lys^{40}, and His^{114}—expected to interact with P_i (*22*) cannot be seen in this type of experiment because of rapid proton exchange with solvent). A-2′-p induced particularly large perturbations of the amide protons of Leu^{115} and the Gln^{12} side chain similar to those produced by P_i (Figure 3b). Thus, the 2′-phosphate group occupies the catalytic P_1 site rather than the subsite (P_2) where the 3′-phosphate group of B_2 purine nucleotides in substrates would normally bind (*13*, *52*). In addition, A-2′-p induced a large perturbation of the His^{114} backbone ^{15}N resonance, whereas the Gln^{117} backbone amide proton did not show appreciable response to binding of this inhibitor.

In contrast, binding of the 3′ and 5′ monophosphate derivatives A-3′-p and pA induced much smaller resonance perturbations of Leu^{115} and His^{114} and somewhat less sizable changes in the Gln^{12} side-chain resonance (Figure 3c,d). Instead, moderate perturbations of the Gln^{117} backbone amide proton (50−70 Hz) and side-chain ^{15}N (∼30 Hz, not shown) resonances appear to be characteristic of the interactions of A-3′-p and pA with Ang. In addition, a number of other residues, including Thr^{44}, Glu^{58}, Gly^{62}, Val^{103}, Val^{104}, and Val^{105}, displayed some response to the binding of one or both of these inhibitors. However, none of these resonance perturbations was as large as those of Leu^{115} and His^{114} induced by A-2′-p (Figure 3b).

Table 1 lists the dissociation constants of P_i, A-2′-p, A-3′-p, and pA along with those of the other nucleotide inhibitors studied, as calculated from the magnitudes of the resonance perturbations for various residues at different inhibitor concentrations. Similar K_D values were derived for each inhibitor irrespective of the resonance used, as long as the residue involved lies within the active site of Ang. These values are in good agreement with the kinetic K_i measurements and indicate that A-2′-p binds ∼3−5 times more effectively than the other monophosphates. K_D values for A-3′-p and pA based on perturbations of Val^{104} and Val^{105}, which interact with the side chains of Leu^{115} and Ile^{119} near the active site, are in the same range as those calculated from the effects on Gln^{12}, Leu^{115}, and Gln^{117}. However, values derived from perturbations of residues well away from the active site (e.g., Glu^{58} and Gly^{62}) are significantly higher. These observations suggest that A-3′-p and pA interact with Ang less specifically than A-2′-p and have alternative binding modes involving regions outside the active site.

Effects of Adding 5′-Phosphate Groups: ^1H and ^{15}N Resonance Perturbations of Ang Residues Induced by pA-2′-p, ppA-2′-p, pA-3′-p, and ppA. Figure 4a,b shows resonance perturbations of Ang induced by saturating amounts of pA-2′-p and ppA-2′-p. Both inhibitors caused dramatic perturbations of residues Leu^{115} (HN), His^{114} (^{15}N), and Gln^{12} (side-chain NH_2), in some cases even greater than with A-2′-p. Thus, induction of large effects on these active site residues appears to be a general feature of all of the 2′-phosphoadenosine-based inhibitors. However, some additional resonance perturbations were observed with pA-2′-p (Ile^{42}, Cys^{81}, Leu^{83}, and Arg^{121}) and ppA-2′-p (Cys^{26}, Ser^{37}, Arg^{51}, Lys^{54}, Asn^{61}, Gly^{62}, and Arg^{122}) that had not been seen with A-2′-p. The K_D values for pA-2′-p and ppA-2′-p calculated from the Leu^{115}, His^{114}, and Gln^{12} perturbations were 6- and 20-fold, respectively, lower than for A-2′-p (Table 1), in excellent agreement with the kinetic data (Figure 1). The values for pA-2′-p derived from perturbations of Arg^{121} and

Table 1: Binding Constants of the Phosphate Ion and Phosphoadenosine-Based Nucleotides Determined through Resonance Perturbations of the Selected Ang Residues

	K_D (mM)						
inhibitor	Leu^{115} H^N	Gln^{12} side-NH_2 syn	His^{114} ^{15}N	Gln^{117} H^N	Arg^{121} H^N	Arg^{122} H^N	Ile^{42} ^{15}N
P_i	~7	~9		~8			
A-2′-p	1.9	2.3	2.0				
A-3′-p	~9	~9		~7			
pA	5.5	5.9		5.1			
pA-2′-p	0.3	0.3	0.3		0.3		0.5
pA-3′-p	1.3	1.2		1.7			1.0
ppA	1.0	1.0		1.9			1.3
ppA-2′-p[a]	0.1	0.1	0.1			0.1	

	K_D (mM)						
inhibitor	Thr^{44} H^N	Glu^{58} ^{15}N	Gly^{62} H^N	Cys^{81} H^N	Leu^{83} H^N	Val^{104} H^N	Val^{105} ^{15}N
A-3′-p	≫10	≫10	≫10			5.5	~7
pA		~8	~9			4.9	5.5
pA-2′-p				0.8	0.8		
pA-3′-p			2.5	1.2	1.3	1.9	2.0
ppA			1.2	1.1	1.3	2.2	1.5

[a] Resonance perturbations for other residues (Cys^{26}, Ser^{37}, Arg^{51}, Lys^{54}, Asn^{61}, Gly^{62}) by ppA-2′-p did not appear to reach plateaus at the inhibitor concentration (6.1 mol excess) yielding the maximal changes of perturbations of Arg^{122} and the three active site residues.

Ile^{42} and for ppA-2′-p from the perturbation of Arg^{122} are comparable to those based on residues Gln^{12}, His^{114}, and Leu^{115}. These observations suggest that the 2′-phosphate of pA-2′-p and ppA-2′-p, like that of A-2′-p, occupies P_1 and that the additional 5′-phosphate and pyrophosphate groups may interact with residues Arg^{121}, Arg^{122}, and Ile^{42}. These residues are in the active site region of Ang, and it has been proposed that Arg^{121} and/or Arg^{122} may form part of a substrate binding site upstream from P_1 (*53*). Distinctly larger K_D values for pA-2′-p and ppA-2′-p were calculated from the other perturbations, all involving residues outside the active site. Thus, these inhibitors also seem to have secondary binding sites.

Addition of a 5′-phosphate to A-3′-p and pA had no major impact on the pattern of resonance perturbations (Figures 3c vs 4c and 3d vs 4d). In both cases, the perturbations of the Leu^{115} and His^{114} backbone NH remained much smaller than those measured with the 2′-phosphoadenosine nucleotides, although a modest increase in the effect on Leu^{115} was seen for ppA versus pA. The 5′-β-phosphate group in ppA enhanced the perturbation of the Gln^{12} side-chain NH_2 protons to the level observed for the A-2′-p series, and the effect on the Gln^{117} backbone NH was somewhat greater for pA-3′-p than for A-3′-p. The presence of the additional 5′-phosphate group induced perturbations of three residues (Ile^{42}, Cys^{81}, and Leu^{83}) not affected appreciably by A-3′-p or pA binding. Again, the K_D values calculated from the perturbations of active site residues (Table 1) were entirely consistent with the kinetic measurements (Figure 1) and showed improvements in binding affinity associated with the phosphate additions (~6-fold in both instances). However, in contrast with the A-2′-p series, some of the K_D values based on residues outside the active site (e.g., Cys^{81} and Leu^{83}) are in the same range, indicating that specific binding to the active site is not as predominant.

Effects of Attaching 2′-Deoxyuridine to ppA-2′-p: Resonance Perturbations of Ang Residues Induced by dUppA-2′-p. Figure 4e shows resonance perturbations of Ang induced by a 6.3-fold molar excess of dUppA-2′-p. No remarkable further perturbations were seen beyond those induced by ppA-2′-p. Large perturbations of the backbone NH resonances of Leu^{115} and His^{114} can be attributed to the A-2′-p portion of the dUppA-2′-p molecule as in the other three 2′-phosphoadenosine nucleotides, A-2′-p, pA-2′-p, and ppA-2′-p (Figures 3b, 4a, and 4b, respectively). Modest perturbations of some other residues (Ser^{37}, Arg^{51}, Lys^{54}, Asn^{61}, and Arg^{122}) are very similar to those caused by the binding of ppA-2′-p. These observations indicate that the dU moiety itself does not interact with the Ang backbone and that binding of the dUppA-2′-p molecule does not have any significant impact on the blockage of the B_1 pyrimidine-binding subsite. The K_D values of dUppA-2′-p estimated from the perturbations of active site residues were similar to those for ppA-2′-p, consistent with results from earlier kinetic studies (ref *13*; Figure 1).

Perturbations of Aromatic Side-Chain Resonances of Ang Induced by the Binding of pA-2′-p and dUppA-2′-p. Interactions of pA-2′-p and dUppA-2′-p with Ang were investigated further to clarify the binding mode of the 2′-phosphoadenosine-based inhibitors. Nucleotides with 3′-phosphate or with only 5′-phosphates were not included in these studies because they bind more weakly and apparently less specifically to Ang. The aromatic regions of the ^{13}C,^{1}H-HSQC spectra for the nucleotide-free and the complexed states of Ang were compared (Figure 5). All the ^{13}C,^{1}H-HSQC signals, except for $^{13}CH^{\epsilon 1}$ of histidines and $^{13}CH^{\zeta}$ of some phenylalanines, were assigned through the C^{β}/H^{δ} and C^{β}/H^{ϵ} resonance connectivities in the (HB)CB(CGCD)HD and (HB)CB(CGCDCE)HE spectra. The His-δ_2 and His-ϵ_1 signals are characterized by unique doublet and singlet patterns in the high-resolution spectra (Figure 5a,b) along the ^{1}H and ^{13}C dimensions, respectively. It is seen that binding of pA-2′-p and dUppA-2′-p perturbed the imidazole δ_2 protons of three histidines (His^{8}, His^{13}, and His^{114}), the ϵ_1 protons of some histidines, the δ-proton of Tyr^{6}, and the δ-proton of Phe^{9} in very similar ways. Among these, the perturbation of the His^{114}-δ_2 proton resonance was particularly large for both inhibitors.

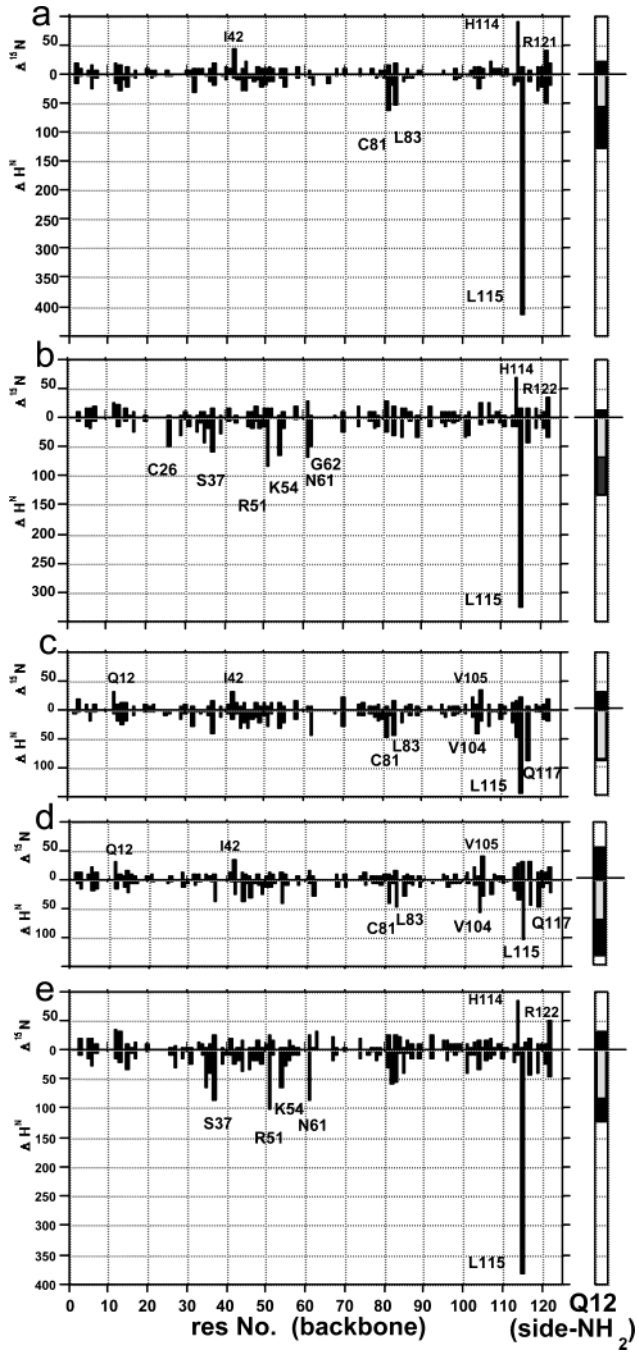

FIGURE 4: Perturbations (in Hz or 500.13 × $|\Delta\delta_H|$ for proton and 50.68 × $|\Delta\delta_H|$ for ^{15}N) for the ^1H and ^{15}N resonances of the backbone amide groups and the side-chain NH_2 group of Gln^{12} of ^{15}N-labeled Ang by (a) pA-2′-p (at 21 mol excess), (b) ppA-2′-p (at 6.1 mol excess), (c) pA-3′-p (at 60 mol excess), (d) ppA (at 60 mol excess), and (e) dUppA-2′-p (at 6.3 mol excess) measured in a buffer of 50 mM sodium acetate containing 0.2 mM EDTA, at pH 5.0 and 298 K. The concentrations of Ang were in the range of 0.1−0.14 mM. The different parts in the bars of the Gln^{12} side chain depict each of the perturbations of the syn (hatched) and anti (black) amine protons of the NH_2 group.

To identify the origin of the resonance perturbation of the His^{114} side chain, NOE contacts involving the His^{114}-δ_2 protons were analyzed in detail for free Ang and for Ang in complex with pA-2′-p and dUppA-2′-p (Figure 6). Assignments of the CH_3 protons of $^{15}N/^{13}C$-labeled Ang were accomplished through a combined analysis of HCCH-TOCSY and HNCACB spectra measured for the three samples. The residues showing NOE contacts with the His^{114}-

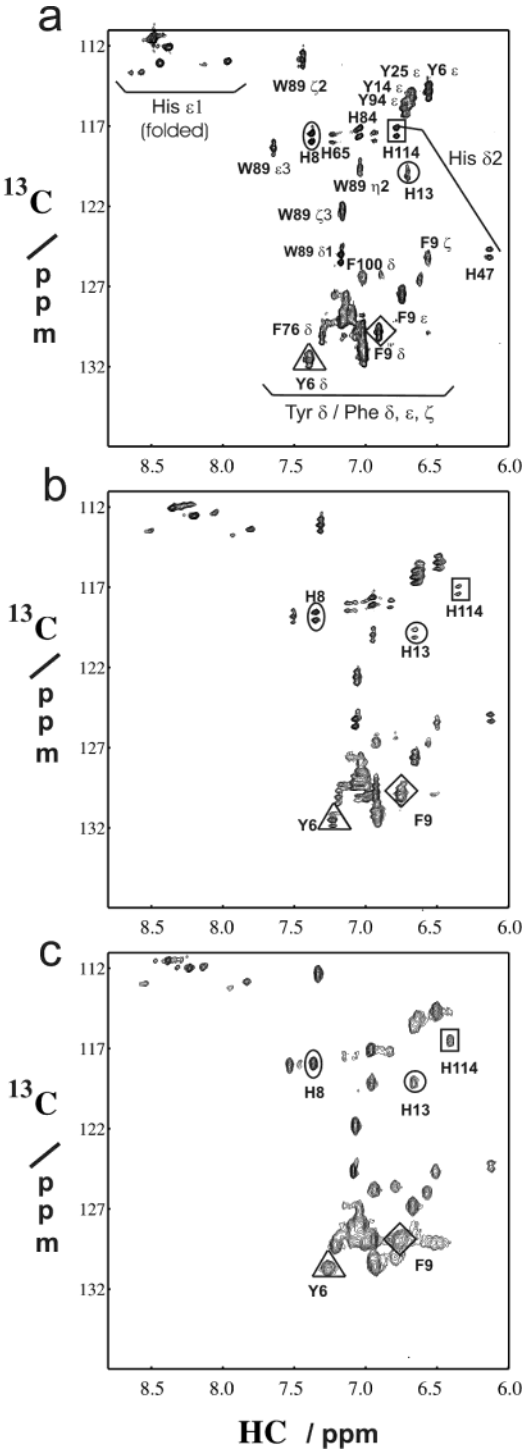

FIGURE 5: 800 MHz aromatic-^{13}C,^1H-HSQC spectra of a $^{15}N/^{13}C$ doubly labeled Ang at a concentration of 1 mM for (a) the nucleotide-free state, (b) a state in the presence of 10 mol excess of pA-2′-p, and (c) a state in the presence of 6.3 mol excess of dUppA-2′-p, in a buffer of 50 mM sodium acetate-d_3 containing 0.2 mM EDTA, at pH 5.0 and 298 K.

δ_2 protons were different for free Ang versus both of the complexes, suggesting that the His^{114} side chain undergoes a conformational change upon binding of pA-2′-p and dUppA-2′-p. Resonance shifts for the His^{114} β-protons from the free state (Figure 6) also indicate a change in the environment around the His^{114} residue when the inhibitors bind.

Three-dimensional structures of Ang have revealed two distinct conformations for the side chain of His^{114}, as had

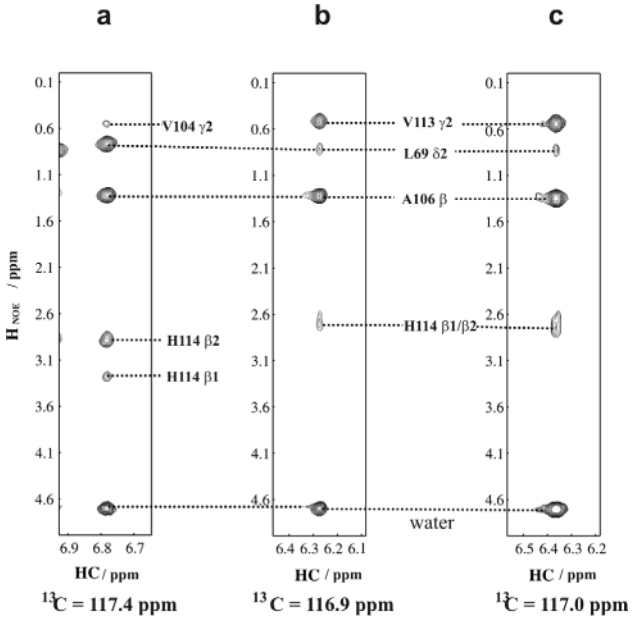

FIGURE 6: 800 MHz NOESY-aromatic ^{13}C,^{1}H-HSQC spectra of 1.0 mM $^{15}N/^{13}C$ doubly labeled Ang. Shown are only strips of the spectra specifying the (^{13}C,^{1}H) resonances of His^{114}-δ_2 (a) for the nucleotide-free state, (b) in the presence of 10 mol excess of pA-2′-p, and (c) in the presence of 6.3 mol excess of dUppA-2′-p, in a buffer of 50 mM sodium acetate-d_3 containing 0.2 mM EDTA, at pH 5.0 and 298 K.

been reported previously (*54*, *55*) for the corresponding residue (His^{119}) of RNase A. The high-resolution X-ray structure of free Ang (*21*) shows only the major A conformation ($\chi_1 \approx 168°$; $\chi_2 \approx 88°$) that predominates in RNase A, whereas the NMR structure of Lequin et al. (*23*) indicates a dynamic equilibrium between this conformation and a minor B conformation ($\chi_1 \approx -60°$; $\chi_2 \approx -65°$). (χ_1 is the torsion angle for N$-$C$^{\alpha}-$C$^{\beta}-$C$^{\gamma}$, and χ_2 is the torsion angle for C$^{\alpha}-$C$^{\beta}-$C$^{\gamma}-$N$^{\delta1}$). In conformation A, the His^{114}-δ_2 proton has short distances to the side-chain CH_3 protons of Leu^{69} that correspond well to the strong NOE connectivity between these protons we observe for free Ang (Figure 6a). In contrast, strong NOE signals between the His^{114}-δ_2 and the Val^{113}-γ-CH_3 protons were observed for both [pA-2′-p]- and [dUppA-2′-p]-bound states of Ang (Figure 6b,c), and the NOE intensities between Leu^{69} and His^{114} greatly decreased. This provides clear evidence that His^{114} adopts the alternative B conformation in both complexes. (The His^{114}-δ_2 and the Ala^{106}-β protons, which show strong NOE signals in free Ang and the two complexes, are separated by nearly identical distances in the two conformations.)

Intraligand and Intermolecular NOEs of pA-2′-p and dUppA-2′-p in Complex with Ang. NOEs originating from free nucleotide protons were collected to obtain further information on the contacts of Ang with pA-2′-p and dUppA-2′-p. These NOESY spectra contain all ^{1}H,^{1}H-correlations of the protons of the nucleotides, including NOEs within the bound nucleotide (transferred NOEs) as well as intermolecular NOEs between the nucleotide and Ang. Assignments of the protons of the two nucleotides, which were used to identify the intranucleotide NOEs and through-bond correlations, were carried out using the ^{1}H,^{1}H-TOCSY and ^{1}H,^{1}H-ROESY spectra of the nucleotides. A total of 10 NOEs were identified as intranucleotide transferred NOEs for the dUppA-2′-p complex (Table 2). The adenine ring H8 proton had NOE contacts with the H1′, H2′, H4′, and H5′ protons of the adenosine sugar moiety, while the adenine ring H2 proton (in the six-membered ring) of dUppA-2′-p did not exhibit any intranucleotide NOEs. These intraligand NOE patterns suggest that the adenine aromatic ring is oriented in such a way that the H2 proton points away from the rest of the nucleotide. Furthermore, the uracil ring H6 proton of dUppA-2′-p had only NOE contacts with the H2′ and H5′ deoxyribose protons of the dU moiety but no NOEs to other parts of the dinucleotide. The intraligand NOEs observed for the pA-2′-p complex were almost identical to those identified within the pA-2′-p portion of the dUppA-2′-p complex (Table 2). Very significantly, neither complex exhibited an intraligand NOE between the adenine H8 proton and the H3′ proton of the adenosine ribose ring, even though NOEs involving other protons of the same sugar moiety were clearly observed (Table 2). These similar patterns of intrali-

Table 2: Intraligand NOEs[a] Observed for pA-2′-p and dUppA-2′-p in Complex with Ang

no.	intensity of NOE	pA-2′-p[b] ^{1}H/ppm	dUppA-2′-p[c] ^{1}H/ppm	assignment (base)
		with adenine ring H8 (8.42 ppm)		
1	strong	5.05	5.00	H2′(A)
2	medium	6.21	6.17	H1′(A)
3	medium	4.09	4.18	H5′(A)
4	weak	4.56	4.57	H4′(A)
5	medium		2.42	H2a′(dU)
6	weak		2.06	H2b′(dU)
		with uracil ring H6 (7.61 ppm)		
7	medium		2.06	H2b′(dU)
8	weak		2.42	H2a′(dU)
9	weak		3.69	H5′(dU)
		with H1′ of deoxyuridine (dU) (6.04 ppm)		
10	weak		4.18	H5′(A)

[a] No NOEs were observed between the adenine H8 ring proton and the clearly resolved H3′ proton of the adenosine ribose ring for both complexes. [b] pA-2′-p was 15 mol excess over ~1 mM $^{15}N/^{13}C$-Ang. [c] dUppA-2′-p was 6 mol excess over ~1 mM $^{15}N/^{13}C$-Ang.

Table 3: Intermolecular NOEs between pA-2′-p and dUppA-2′-p Protons and ^{13}C-Attached Protons of $^{15}N/^{13}C$-Labeled Ang

		Ang resonance (ppm)		
no.	intensity of NOE signal	[pA-2′-p][a] ^{1}H (^{13}C)	[dUppA-2′-p][b] ^{1}H (^{13}C)	assignment
		with adenine ring H2 (8.13 ppm)		
1	strong	1.31 (19.4)	1.31 (19.4)	Ala^{106} H$^{\beta}$
2	strong	0.83 (21.4)	0.80 (21.2)	Leu^{69} H$^{\delta2}$
3	weak	ND[c] (23.3)	ND[c] (23.2)	(Leu^{69}H$^{\delta1}$)[d]
4	weak	1.38 (41.4)	ND[c] (ND[e])	(Leu^{69} H$^{\beta2}$)[d]
5	weak	ND[c] (30.2)	ND[c] (ND[e])	(His^{114} H$^{\beta2}$)[d]
6	weak	ND[c] (39.7)	ND[c] (ND[e])	unknown[f]
		with ribose H1′ (6.17 ppm)		
7	medium	2.78 (30.2)	2.72 (30.3)	His^{114} H$^{\beta2}$
8	weak	1.38 (41.4)	ND[c] (41.7)	(Leu^{69} H$^{\beta2}$)[d]
9	weak	ND[c] (52.0)	ND[c] (ND[e])	(Leu^{69} H$^{\alpha}$)[d]
		with uracil ring H5 (5.70 ppm)		
10	weak		1.71 (ND[e])	(Arg^{66} H$^{\beta1}$/ Arg^{121} H$^{\beta2}$)[d]
11	weak		0.48 (ND[e])	unknown[f]

[a] In the presence of 10 mol excess of pA-2′-p. [b] In the presence of 6 mol excess of dUppA-2′-p. [c] ND: proton signals were not detected. [d] Assignments compatible with uniquely assigned intermolecular NOEs (nos. 1, 2, and 7). [e] ND: ^{13}C signal was not detected. [f] No assignments were compatible with other assigned intermolecular NOEs.

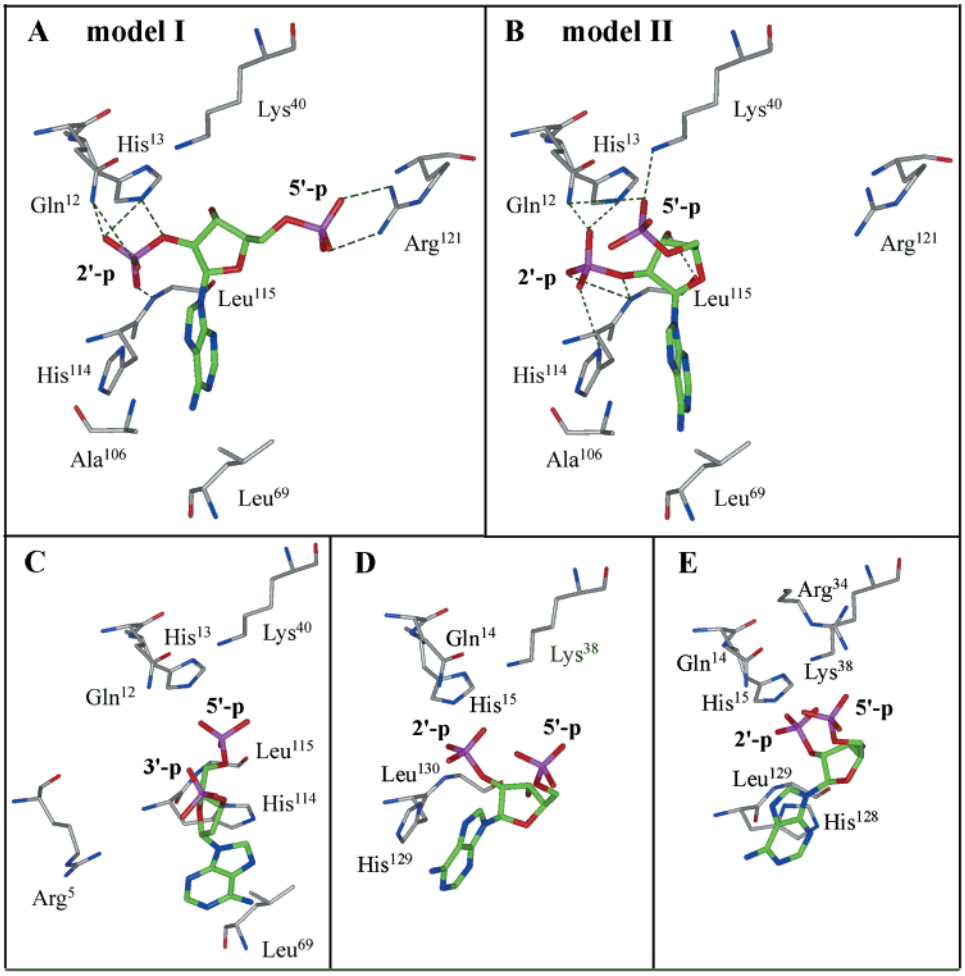

FIGURE 7: (A) Model I: the lowest energy structural model of the Ang-[pA-2′-p] complex derived by using AutoDock 3.0.5. All possible hydrogen bonds for the modeled complex are shown as dashed lines. (B) Model II: a minor alternative docking solution obtained only when the inhibitor was given a C2′*endo*/C3′*exo* ribose pucker. (C) Expected binding mode of substrates to Ang based on a superposition of the crystal structure of free Ang (PDB code 1B1I) with that of the RNase A-d(ApTpApA) complex (ref *52*; PDB code 1RCN). Only the pA-3′-p portion of the substrate analogue on the immediate 3′ side of thymidine is shown. (D) Crystal structure of the complex of EDN with pA-2′-p (ref *50*; PDB code 1HI3). (E) Crystal structure of the complex of ECP with pA-2′-p (ref *62*; PDB code 1H1H). The complexes are rendered in stick display mode (Insight II) with standard atomic colors, using green for ligand carbons and gray for protein carbons.

gand transferred NOEs for pA-2′-p and dUppA-2′-p indicate that the adenosine mononucleotide moieties of both nucleotides have similar bound conformations in complex with Ang.

Additional NOESY measurements (see Materials and Methods) were made to assign Ang residues involved in intermolecular NOEs with pA-2′-p and dUppA-2′-p. These spectra provided resonance locations of Ang ^{13}C atoms, each of which is attached to an Ang proton that gives rise to an intermolecular NOE with a proton of the bound nucleotide. Nine cross-peaks were identified as intermolecular NOEs between pA-2′-p and Ang (Table 3). Of these, three signals were unambiguously assigned to Ang residues with unique (^{13}C, ^{1}H) resonance frequencies. In particular, the adenine H2 proton exhibited two strong NOEs with the methyl protons of Leu^{69} and Ala^{106}, and the ribose H1′ proton had an NOE with a β-proton of the His^{114} side chain (Table 3). Five of the six weaker NOE signals could also be conditionally assigned to Leu^{69} or His^{114} protons, guided by the uniquely assigned intermolecular NOEs. For the dUppA-2′-p complex, similar intermolecular NOEs involving adenosine protons were assigned to the same Ang residues as for pA-2′-p (Table 3), providing further evidence that Ang binds to the pA-2′-p moiety of dUppA-2′-p in the same way as to pA-2′-p itself. Two weak NOEs involving the uracil ring H5 proton could be assigned to a β-proton of either Arg^{66} or Arg^{121}, but there are no intermolecular NOE contacts of the dU moiety with Ang residues around the B_1 site, consistent with resonance perturbation data suggesting that the dU portion of dUppA-2′-p does not occupy this subsite.

Docking Analysis of the Bound Conformations of pA-2′-p and dUppA-2′-p in Complex with Ang. To explore possible conformations and orientations of pA-2′-p and dUppA-2′-p bound to Ang, pA-2′-p was docked onto Ang with AutoDock 3.0.5 (*49*), and a model for the dUppA-2′-p complex was manually generated from the predominant docking pose using energy minimization. The crystal structure of free Ang was used to model high-resolution structures of the complexes since NOEs of free Ang in solution show the absence of major structural changes. Moreover, three-dimensional structure models of Ang calculated using NMR shifts and NOEs of the Ang-[dUppA-2′-p] complex showed minimal deviations from the global fold structure of free Ang determined here and reported previously (results not shown). However, as discussed above, NOEs involving the His^{114}-δ_2 proton in the Ang-[pA-2′-p] or Ang-[dUppA-2′-p] complexes indicate

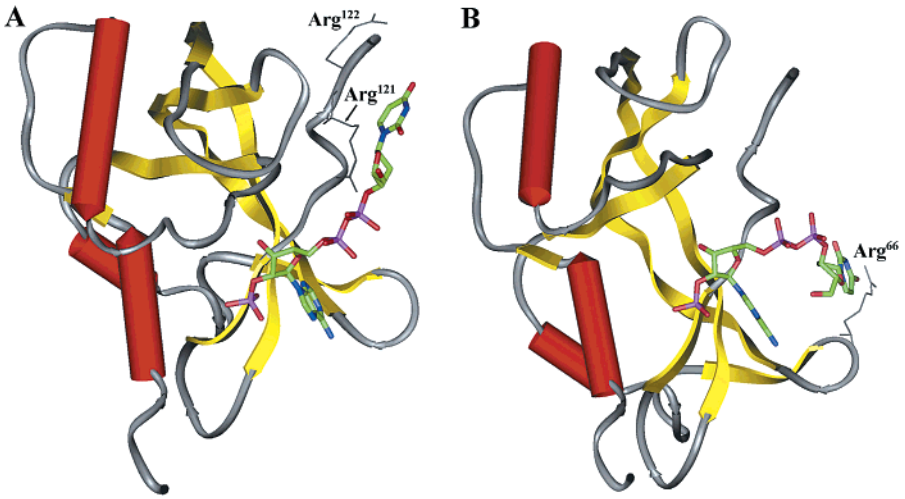

FIGURE 8: Possible dUppA-2′-p orientations in complex with Ang that are consistent with the observed intermolecular NOEs. (A) dUppA-2′-p configuration with uracil H5 near Arg^{121} H$^{\beta 2}$. (B) dUppA-2′-p configuration with uracil H5 near Arg^{66} H$^{\beta 1}$.

that the side chain of His^{114} assumes a conformation different from that observed in the crystal structure (B vs A). The docking analyses, therefore, utilized both conformations (with χ_1 and $\chi_2 = -65°$ for B, as in the complex of EDN with pA-2′-p; ref *50*). In addition, the χ_3 torsion angle of the Gln^{12} side chain ($C^{\beta}-C^{\gamma}-C^{\delta}-N^{\epsilon 2}$) was changed from 107 to −76° so that the NH_2 group would be oriented toward P_1, as in the high-resolution X-ray structure of the Ang−P_i complex (*22*). Furthermore, we used two pA-2′-p structures that differ with respect to the puckering of the ribose ring (C2′*endo*/C3′*exo* and C3′*endo*, as commonly seen in complexes of other RNases with adenosine nucleotides (*50*, *51*)); this was necessary because AutoDock itself cannot alter ring conformations, although it allows full flexibility around rotatable bonds in ligands.

None of the docking solutions for pA-2′-p obtained with His^{114} in conformation A were compatible with the present NMR observations. For example, in all generated positions, the adenine H2 of pA-2′-p is far from the methyl groups of Ang Ala^{106} and Leu^{69} (6.5−15.5 and 9.8−15.1 Å, respectively). Further, in some cases, the 2′-phosphate of pA-2′-p is too far from the amide proton of Ang Leu^{115} to form a hydrogen bond (4.8−10.6 Å), inconsistent with the large resonance perturbation of this proton by the nucleotide inhibitor (Figure 4a). In contrast, the solutions found when His^{114} is assigned to the B conformation were able to satisfy all of the constraints from the experimental data, and the estimated binding energies were 2−3 orders of magnitude lower than those calculated when His^{114} was in the standard A conformation. In the lowest-energy ligand positions, oxygens of the 2′-phosphate group of pA-2′-p are placed within hydrogen-bonding distance from the Leu^{115} backbone NH, Gln^{12} side-chain NH_2, and His^{13} imidazole NH$^{\epsilon 2}$, and the adenine ring of pA-2′-p forms stacking interactions with the imidazole ring of His^{114} (Figure 7A) (the hydrogen bond criteria used are donor−acceptor distance <3.4 Å and donor−hydrogen−acceptor angle >90°). The adenine aromatic ring of the docked pA-2′-p points away from the adenosine sugar moiety as predicted from intraligand transferred NOEs (Table 2). The ribose pucker for this docked pA-2′-p turned out to be C2′*endo*/C3′*exo*, which is in exact agreement with the patterns of intraligand NOEs, especially the absence of a transferred NOE between the adenine H8 proton and the H3′ proton of the ribose ring (vide supra). Moreover, the adenine H2 and the ribose H1′ of pA-2′-p are near the side chains of Leu^{69}, Ala^{106}, and His^{114}, in agreement with the intermolecular NOEs (Table 3). Importantly, all of the pA-2′-p docking solutions that are consistent with the NMR observations place the 2′-phosphate in the P_1 subsite, whereas the 5′-phosphate would occupy P_1 if the inhibitor binds in a manner analogous to normal RNA substrates (ref *52*; Figure 7C).

Two reasonable configurations with this alternative pA-2′-p binding mode were found that were nearly identical except with respect to the orientation of the 5′-phosphate group. In the predominant docking solution (model I, Figure 7A), the 5′-phosphate group points toward the C-terminal of Ang and forms hydrogen bonds with the Arg^{121} side chain. In some of the solutions obtained for pA-2′-p with the C2′*endo*/C3′*exo* ribose pucker (model II, Figure 7B), the 5′-phosphate group of pA-2′-p instead forms hydrogen bonds with the side chains of Gln^{12} and Lys^{40}.

A potential binding mode for dUppA-2′-p was investigated by grafting dUp onto the 5′-phosphate of pA-2′-p in model I (model II is incompatible with the NOE between uracil and Arg^{66} or Arg^{121} of Ang). Retention of the orientation of pA-2′-p seemed reasonable in light of the nearly identical resonance perturbations and intraligand and intermolecular NOEs for the pA-2′-p and dUppA-2′-p complexes. Manual rotation of the dUp portion of the inhibitor showed that uracil H5 could be placed within 5 Å of either Arg^{121} H$^{\beta 2}$ (Figure 8A) or Arg^{66} H$^{\beta 1}$ (Figure 8B), consistent with intermolecular NOEs (Table 3). The bent conformation for dUppA-2′-p (Figure 8B) is supported by the intraligand NOEs between the adenosine and the deoxyribose (dU) moieties (Table 2). It is noteworthy that all unstrained positions for the uracil moiety project away from the protein into the solvent and are far from the normal B_1 subsite utilized by substrates.

DISCUSSION

Ang favors adenine as the nucleobase in the B_2 position of substrates (*9*, *56*), and studies on nucleotide inhibitors of Ang have therefore focused primarily on adenosine derivatives. Although all of the inhibitors examined bind much less avidly to Ang than to RNase A, a wide range of affinities

(from ~14 to 0.1 mM) has been observed, and some clear preferences have emerged. Within the series of compounds examined here, the order of affinities, based on both kinetic determinations and NMR titrations, is ppA-2′-p ~ dUppA-2′-p > pA-2′-p > ppA > pA-3′-p > A-2′-p > pA > P_i > A-3′-p (Figure 1 and Table 1). In all cases, derivatives with a 2′-phosphate bind severalfold more tightly than the corresponding 3′-phosphate isomer. (This also applies to ppA-2′-p vs ppA-3′-p, a nucleotide not examined here but included in a previous kinetic study (*14*).)

The interactions of Ang with the various inhibitors can be evaluated by comparing the patterns and extents of proton and ^{15}N resonance perturbations of Ang residues induced upon binding (Figures 3 and 4). Binding of the 3′-phosphoadenosine-based nucleotides and 5′-phosphoadenosines causes modest resonance perturbations of many Ang residues both within and outside the active site. In contrast, 2′-phosphoadenosine-based nucleotides all induce characteristically large resonance perturbations of the three Ang residues Leu^{115}, Gln^{12}, and His^{114}. Therefore, Ang appears to bind the 2′-phosphoadenosine nucleotides basically in the same manner and through interactions more specific than those for the binding of 3′- and 5′-phosphoadenosine nucleotides. The Leu^{115} and Gln^{12} groups affected (backbone amide NH and side-chain NH_2) are among those seen to be involved in hydrogen bonds with P_i in the crystal structure of the Ang−P_i complex (*22*), along with others (the His^{13} and His^{114} imidazoles and Lys^{40} ammonium group) not visualized in this NMR experiment. Binding of P_i also induces resonance perturbations of these residues (Figure 3a), suggesting that the binding mode in solution is similar. However, P_i does not influence the His^{114} main-chain ^{15}N resonance, indicating that the perturbation induced by the 2′-phosphoadenosine nucleotides may not be simply due to an interaction of the 2′-phosphate with the side chain of His^{114}.

Indeed, significant resonance perturbations of the side-chain protons of His^{114} indicate that the conformation of this residue changes upon binding of pA-2′-p or dUppA-2′-p (Figures 5 and 6). Characteristic NOEs between the His^{114}-δ_2 proton and other residues of Ang in complexes with pA-2′-p and dUppA-2′- p (Figure 6) show that the His^{114} side chain has rotated about the $C^{\alpha}-C^{\beta}$ and $C^{\beta}-C^{\gamma}$ bonds into the nonstandard B conformation. (The $C^{\alpha}-C^{\beta}$ rotation is demonstrated by the gain of NOEs involving Val^{113} and loss of NOEs involving Leu^{69}; the maintenance of the strong NOEs with Ala^{106} despite this change in orientation implies that the $C^{\beta}-C^{\gamma}$ rotation has also occurred.) This conformational change also explains the large perturbations of the ^{15}N resonance of the His^{114} backbone caused by the 2′-phosphoadenosine nucleotides. In the B conformation, the main-chain ^{15}N atom of His^{114} is placed in a region where the shielding effect of the His^{114} imidazole ring would endow this atom with a more upfield-shifted ^{15}N resonance (*57*). Moreover, computational docking of pA-2′-p to Ang produces structures consistent with the observed intermolecular NOEs and other NMR data only when His^{114} takes the B conformation. The docking models show that the His^{114} imidazole side chain in this conformation stacks with the adenine ring of the inhibitor (Figure 7A,B) and contributes entirely as a base-binding residue (B_2) rather than participating in phosphate binding at P_1.

The NMR data and modeling studies reveal that pA-2′-p and the pA-2′-p moiety of dUppA-2′-p bind to Ang in an orientation that differs strikingly from that predicted in earlier studies, most notably in that the 2′-phosphate rather than the 5′-phosphate occupies the P_1 subsite. Comparison of perturbations for pA-2′-p versus A-2′-p (Figure 4a vs 3b) indicates that the 5′-phosphate affects the Arg^{121} backbone amide group. Addition of another phosphate to the 5′-position instead caused resonance perturbations of Arg^{122} (Figure 4b). A comparable ^{15}NH resonance perturbation is also seen for Arg^{122} in the complex of Ang with dUppA-2′-p (Figure 4e). Therefore, it seems likely that the 5′-phosphate groups of pA-2′-p, ppA-2′-p, and dUppA-2′-p extend toward the C-terminal region, forming hydrogen bonds and/or Coulombic interactions with the positively charged Arg^{121}−Arg^{122} unique to Ang, as in the major docking model for pA-2′-p (model I, Figure 7A). All the structure models show a common binding mode for the adenosine core structure, with the adenine moiety lying on the periphery of the putative B_2 subsite and making aromatic interactions with the side chain of His^{114} in the B conformation.

Crystal structures of complexes of RNase A with the 3′,5′-pyrophosphate-linked dinucleotides pdUppA-3′-p and dUppA show a substrate-like binding mode with the uracil ring in B_1 and the 3′,5′-pyrophosphate in P_1 (*30*, *58*). It was anticipated that dUppA-2′-p would interact with Ang analogously, which in this case would require reorientation of the C-terminal segment containing Gln^{117} to provide access to B_1. However, NMR data establish that in fact the dinucleotide binds to Ang in an entirely different manner. There are no significant perturbations of backbone NH resonances for Ang residues 116−120 upon addition of dUppA-2′-p, demonstrating that the conformation of this segment has not been altered appreciably. Intramolecular (Ang) and intermolecular NOEs indicate that the pA-2′-p portion of dUppA-2′-p is oriented with the 2′-phosphate in P_1. Moreover, the dU moiety has no NOEs with residues in the B_1 site of Ang and only weak NOEs with residues distant from this site, suggesting that it largely extends away from the surface of the protein.

No three-dimensional structure has been reported for the complex of pA-2′-p with RNase A, but the crystal structure of the RNase A-[ppA-2′-p] complex (*51*) shows that the 5′-pyrophosphate group is placed in the P_1 site, the adenine is in B_2, the 2′-phosphate is in P_2, and the side chain of His^{119} (corresponding to His^{114} of Ang) adopts the standard A conformation. The difference between the interactions of the 2′-phosphoadenosine mononucleotides with Ang and RNase A may be explained in part by the marked differences in the B_2 subsite architecture. In RNase A, the side chains of Asn^{67}, Gln^{69}, Asn^{71}, and Glu^{111} surround the adenine ring, forming multiple hydrogen bonds and providing a highly constrained environment (*59*−*61*). In this position, the adenine is also able to make stacking interactions with the His^{119} imidazole in its A conformation. Ang contains no structural analogues of the RNase A residues Asn^{67}, Gln^{69}, Asn^{71} and has a much less defined B_2 subsite. Thus, the positioning of adenosine nucleotides within the Ang active site may be largely driven by optimization of the interactions of the phosphate(s) as well as the ring stacking interactions between adenine and the rotated His^{114} side chain.

Recently determined crystal structures of the complexes of pA-2′-p with two other RNases, EDN and eosinophil

cationic protein (ECP), both show the 2′-phosphate in P_1 as in the Ang complex. The EDN complex (ref *50*, Figure 7D) is similar to the docking models for Ang. Gln^{14} and Leu^{130} of EDN are hydrogen bonded to the 2′-phosphate as for the corresponding Ang residues (Gln^{12} and Leu^{115}), and the side chain of His^{129} is again in the B conformation, where it is almost parallel to and stacks with the adenine ring. However, the 5′-phosphate group of the bound pA-2′-p forms different interactions in the two cases: a water-mediated hydrogen bond with the Met^0 residue of EDN versus a direct contact with the Arg^{121} side chain of Ang (in model I). Neither Met^0 of EDN nor Arg^{121} of Ang has a structural analogue in the other protein. (EDN has a two-residue N-terminal extension as compared to Ang and terminates four residues earlier.) The conformation of pA-2′-p when bound to ECP (ref *62*; Figure 7E) is generally similar to that in the Ang and EDN complexes, but the position of the nucleotide is shifted by a few angstroms. Consequently, the 2′-phosphate oxygens are too far from the backbone nitrogen atom of Leu^{129} (corresponding to Leu^{115} of Ang) to form a hydrogen bond and instead interact with the ammonium group of Lys^{38} (corresponding to Lys^{40} of Ang). The 5′-phosphate extends into the P_{-1} phosphate-binding subsite of ECP, where it hydrogen bonds with the $N^{\eta 2}$ of Arg^{34}. Importantly, His^{128} of ECP adopts the standard A conformation instead of the B conformation observed for His^{114} of Ang and His^{129} of EDN.

In summary, heteronuclear and multidimensional NMR spectroscopy have been used to determine for the first time the three-dimensional structures of Ang complexes with nucleotide inhibitors. The interactions of dUppA-2′-p and pA-2′-p with Ang highlight (i) negatively charged moieties such as phosphates strategically located to form electrostatic contacts with side- and main-chain nitrogens on Ang, (ii) aromatic stacking interactions of the adenine ring of the inhibitors, and (iii) the strength of obstructive interactions preventing the dU moiety of the dinucleotide dUppA-2′-p from reaching the B_1 site. The complexes examined involve two of the most avid nucleotide inhibitors of Ang identified to date, pA-2′-p and dUppA-2′-p, and thus represent a potentially important advance toward the development of more effective antitumor agents targeting the ribonucleolytic active site of Ang. Rational design efforts based on these compounds must now be redirected in light of the unexpected binding mode observed, which would seem to identify the 2′- rather than the 5′-end of the molecule as most promising for modifications to improve affinity.

ACKNOWLEDGMENT

We thank Dr. Zhigang Chen for providing ^{15}N,^{1}H-HSQC spectra of Ang in the presence of the ppA-2′-p and dUppA-2′-p nucleotides and Jan Walter for backbone resonance assignments of free angiogenin. We also thank Michael Brady and Cecilia Roh for excellent technical assistance, Dr. Bert L. Vallee for advice and support, and Dr. James F. Riordan for helpful discussions.

REFERENCES

1. Fett, J. W., Strydom, D. J., Lobb, R. R., Alderman, E. M., Bethune, J. L., Riordan, J. F., and Vallee, B. L. (1985) Isolation and characterization of angiogenin, an angiogenic protein from human carcinoma cells, *Biochemistry 24*, 5480−5486.
2. Strydom, D. J., Fett, J. W., Lobb, R. R., Alderman, E. M., Bethune, J. L., Riordan, J. F., and Vallee, B. L. (1985) Amino acid sequence of human tumor derived angiogenin, *Biochemistry 24*, 5486−5494.
3. Shimoyama, S., Gansauge, F., Gansauge, S., Negri, G., Oohara, T., and Beger, H. G. (1996) Increased angiogenin expression in pancreatic cancer is related to cancer aggressiveness, *Cancer Res. 56*, 2703−2706.
4. Shimoyama, S., Yamasaki, K., Kawahara, M., and Kaminishi, M. (1999) Increased serum angiogenin concentration in colorectal cancer is correlated with cancer progression, *Clin. Cancer Res. 5*, 1125−1130.
5. Hartmann, A., Kunz, M., Kostlin, S., Gillitzer, R., Toksoy, A., Brocker, E. B., and Klein, C. E. (1999) Hypoxia-induced up-regulation of angiogenin in human malignant melanoma, *Cancer Res. 59*, 1578−1583.
6. Olson, K. A., Byers, H. R., Key, M. E., and Fett, J. W. (2001) Prevention of human prostate tumor metastasis in athymic mice by antisense targeting of human angiogenin, *Clin. Cancer Res. 7*, 3598−3605.
7. Olson, K. A., Byers, H. R., Key, M. E., and Fett, J. W. (2002) Inhibition of prostate carcinoma establishment and metastatic growth in mice by an antiangiogenin monoclonal antibody, *Int. J. Cancer 98*, 923−929.
8. Shapiro, R., Riordan, J. F., and Vallee, B. L. (1986) Characteristic ribonucleolytic activity of human angiogenin, *Biochemistry 25*, 3527−3532.
9. Harper, J. W., and Vallee, B. L. (1989) A covalent angiogenin/ribonuclease hybrid with a fourth disulfide bond generated by regional mutagenesis, *Biochemistry 28*, 1875−1884.
10. Shapiro, R., Fox, E. A., and Riordan, J. F. (1989) Role of lysines in human angiogenin: chemical modification and site-directed mutagenesis, *Biochemistry 28*, 1726−1732.
11. Shapiro, R., and Vallee, B. L. (1989) Site-directed mutagenesis of histidine-13 and -114 of human angiogenin. Alanine derivatives inhibit angiogenin-induced angiogenesis, *Biochemistry 28*, 7401−7408.
12. Curran, T. P., Shapiro, R., and Riordan, J. F. (1993) Alteration of the enzymatic specificity of human angiogenin by site-directed mutagenesis, *Biochemistry 32*, 2307−2313.
13. Russo, N., Acharya, K. R., Vallee, B. L., and Shapiro, R. (1996) A combined kinetic and modeling study of the catalytic center subsites of human angiogenin, *Proc. Natl. Acad. Sci. U.S.A. 93*, 804−808.
14. Russo, N., Acharya, K. R., and Shapiro, R. (2001) Small molecule inhibitors of RNase A and related enzymes, *Methods Enzymol. 341*, 629−648.
15. Kao, R. Y. T., Jenkins, J. L., Olson, K. A., Key, M. E., Fett, J. W., and Shapiro, R. (2002) A small-molecule inhibitor of the ribonucleolytic activity of human angiogenin that possesses antitumor activity, *Proc. Natl. Acad. Sci. U.S.A. 99*, 10066−10071.
16. Richards, F. M., and Wyckoff, H. W. (1971) Bovine pancreatic ribonuclease, *Enzymes* (*3rd ed.*) *4*, 647−806.
17. Riordan, J. F. (1997) Structure and function of angiogenin, in *Ribonucleases: Structures and Functions* (D'Alessio, G., and Riordan, J. F., Eds.) pp 445−489, Academic Press, New York.
18. Sorrentino, S., and Libonati, M. (1994) Human pancreatic-type and nonpancreatic-type ribonucleases: A direct side-by-side comparison of their catalytic properties, *Arch. Biochem. Biophys. 312*, 340−348.
19. Boix, E. (2001) Eosinophil cationic protein, *Methods Enzymol. 341*, 287−305.
20. Acharya, K. R., Shapiro, R., Allen, S. C., Riordan, J. F., and Vallee, B. L. (1994) Crystal structure of human angiogenin reveals the structural basis for its functional divergence from ribonuclease, *Proc. Natl. Acad. Sci. U.S.A. 91*, 2915−2919.
21. Leonidas, D. D., Shapiro, R., Allen, S. C., Subbarao, G. V., Veluraja, K., and Acharya, K. R. (1999) Refined crystal structures of native human angiogenin and two active site variants: implications for the unique functional properties of an enzyme involved in neovascularization during tumor growth, *J. Mol. Biol. 285*, 1209−1233.
22. Leonidas, D. D., Chavali, G. B., Jardine, A. M., Li, S., Shapiro, R., and Acharya, K. R. (2001) Binding of phosphate and pyrophosphate ions at the active site of human angiogenin as revealed by X-ray crystallography, *Protein Sci. 10*, 1669−1676.
23. Lequin, O., Thuring, H., Robin, M., and Lallemand, J.-Y. (1997) Three-dimensional solution structure of human angiogenin determined by ^{1}H, ^{15}N NMR spectroscopy—nuclear magnetic resonance

spectroscopy−characterization of histidine protonation states and pK_a values, *Eur. J. Biochem. 250*, 712−726.

24. Richards, F. M., and Wyckoff, H. M. (1973) Ribonuclease-S, in *Atlas of Molecular Structures in Biology* (Phillips, D. C., and Richards, F. M., Eds.) Vol. 1, pp 2−73, Clarendon Press, Oxford, UK.
25. Wlodawer, A., Svensson, L. A., Sjolin, L., and Gilliland, G. L. (1988) Structure of phosphate-free ribonuclease A refined at 1.26 Å, *Biochemistry 27*, 2705−2717.
26. Shapiro, R. (1998) Structural features that determine the enzymatic potency and specificity of human angiogenin: threonine-80 and residues 58−70 and 116−123, *Biochemistry 37*, 6847−6856.
27. Russo, N., Shapiro, R., and Vallee, B. L. (1997) 5′-Diphosphoadenosine 3′-phosphate is a potent inhibitor of bovine pancreatic ribonuclease A, *Biochem. Biophys. Res. Commun. 231*, 671−674.
28. Russo, N., and Shapiro, R. (1999) Potent inhibition of mammalian ribonucleases by 3′,5′-pyrophosphate-linked nucleotides, *J. Biol. Chem. 274*, 14902−14908.
29. Kumar, K., Jenkins, J. L., Jardine, A. M., and Shapiro, R. (2003) Inhibition of mammalian ribonucleases by endogenous adenosine dinucleotides, *Biochem. Biophys. Res. Commun. 300*, 81−86.
30. Jardine, A. M., Leonidas, D. D., Jenkins, J. L., Park, C., Raines, R. T., Acharya, K. R., and Shapiro, R. (2001) Cleavage of 3′,5′-pyrophosphate-linked dinucleotides by ribonuclease A and angiogenin, *Biochemistry 40*, 10262−10272.
31. Shapiro, R., Harper, J. W., Fox, E. A., Jansen, H.-W., Hein, F., and Uhlmann, E. (1988) Expression of Met-(-1) angiogenin in *Escherichia coli*: conversion to the authentic <Glu-1 protein, *Anal. Biochem. 175*, 450−461.
32. Ho, S. N., Hunt, H. D., Horton, R. M., Pullen, J. K., and Pease, L. R. (1989) Site-directed mutagenesis by overlap extension using the polymerase chain reaction, *Gene 77*, 51−59.
33. Studier, F. W., Rosenberg, A. H., Dunn, J. J., and Dubendorff, J. W. (1990) Use of T7 RNA polymerase to direct expression of cloned genes, *Methods Enzymol. 185*, 60−89.
34. Chen, C.-Z., and Shapiro, R. (1997) Site-specific mutagenesis reveals differences in the structural bases for tight binding of RNase inhibitor to angiogenin and RNase A, *Proc. Natl. Acad. Sci. U.S.A. 94*, 1761−1766.
35. Sambrook, J., Fritsch, E. F., and Maniatis, T. (1989) *Molecular Cloning: A Laboratory Manual, 2nd ed.*, Cold Spring Harbor Laboratory Press, Woodbury, NY.
36. Holloway, D. E., Hares, M. C., Shapiro, R., Subramanian, V., and Acharya, K. R. (2001) High-level expression of three members of the murine angiogenin family in *Escherichia coli* and purification of the recombinant proteins, *Protein Expression Purif. 22*, 307−317.
37. Sklenar, V., Piotto, M., Leppik, R., and Saudek, V. (1993) Gradient-tailored water suppression for ^{1}H-^{15}N HSQC experiments optimized to retain full sensitivity, *J. Magn. Reson. 102*, 241−245.
38. Delaglio, F., Gizesiek, S., Vuister, G. W., Zhu, G., Pfeifer, J., and Bax, A. (1995) NMRPipe: a multidimensional spectral processing system based on UNIX pipes, *J. Biomol. NMR 6*, 277−293.
39. Sattler, M., Schleucher, J., and Griesinger, C. (1999) A heteronucler multidimensional NMR experiment for the structure determination of proteins in solution employing pulsed field gradients, *Prog. NMR Spectrosc. 34*, 93−158.
40. Kay, L. E., Xu, G. Y., Singer, A. U., Muhandiram, D. R., and Forman-Kay, J. D. (1993) A gradient-enhanced HCCH-TOCSY experiment for recording side-chain ^{1}H and ^{13}C correlations in H_2O samples of proteins, *J. Magn. Reson. B101*, 333−337.
41. Marion, D., Kay, L. E., Sparks, S. W., Torchia, D. A., and Bax, A. D. (1989) Three-dimensional heteronuclear NMR of nitrogen-15 labeled proteins, *J. Am. Chem. Soc. 111*, 1515−1517.
42. Shaka, A. J., Barker, P. B., and Freeman, R. (1985) Computer-optimized decoupling scheme for wideband applications and low-level operation, *J. Magn. Reson. 64*, 547−552.
43. McCoy, M. A., and Muller, L. (1992) Selective shaped pulse decoupling in NMR: Homonuclear [^{13}C] carbonyl decoupling, *J. Am. Chem. Soc. 114*, 2108−2112.
44. Ikura, M., and Bax, A. D. (1992) Isotope-filtered 2-D NMR of a protein−peptide complex: Study of a skeletal muscle myosin light chain kinase fragment bound to calmodulin, *J. Am. Chem. Soc. 114*, 2433−2440.
45. Nilges, M. (1995) Calculation of protein structures with ambiguous distance restraints. Automated assignment of ambiguous NOE cross-peaks and disulfide connectivities, *J. Mol. Biol. 245*, 645−660.
46. Nilges, M., Macias, M. J., O'Donoghue, S. I., and Oschkinat, H. (1997) Automated NOESY interpretation with ambiguous distance restraints: The refined solution NMR structure of the pleckstrin homology domain from β-spectrin, *J. Mol. Biol. 269*, 408−422.
47. Vranken, W., Tolkachev, D., Xu, P., Tanha, J., Chen, Z., Narang, S., and Ni, F. (2002) Solution structure of a llama single-domain antibody with hydrophobic residues typical of the VH/VL interface, *Biochemistry 41*, 8570−8579.
48. Wishart, D. S., and Sykes, B. D. (1994) The ^{13}C Chemical-Shift Index: A simple method for the identification of protein secondary structure using ^{13}C chemical-shift data, *J. Biomol. NMR 4*, 171−180.
49. Morris, G. A., Goodsell, D. S., Halliday, R. S., Huey, R., Hart, W. E., Belew, R. K., and Olson, A. J. (1999) Automated docking using a Lamarckian genetic algorithm and an empirical binding free energy function, *J. Comput. Chem. 19*, 1639−1662.
50. Leonidas, D. D., Boix, E., Prill, R., Suzuki, M., Turton, R., Minson, K., Swaminathan, J., Youle, R. J., and Acharya, K. R. (2001) Mapping the ribonucleolytic active site of eosinophil-derived neurotoxin (EDN), *J. Biol. Chem. 276*, 15009−15017.
51. Leonidas, D. D., Shapiro, R., Irons, L. I., Russo, N., and Acharya, K. R. (1997) Crystal structures of ribonuclease A complexes with 5′-diphosphoadenosine 3′-phosphate and 5′-diphosphoadenosine 2′-phosphate at 1.7 Å resolution, *Biochemistry 36*, 5578−5588.
52. Fontecilla-Camps, J. C., de Llorens, R., le Du, M. H., and Cuchillo, C. M. (1994) Crystal structure of ribonuclease A·d(ApTpApApG) complex. Direct evidence for extended substrate recognition, *J. Biol. Chem. 269*, 21526−21531.
53. Russo, N., Nobile, V., Di Donato, A., Riordan, J. F., and Vallee, B. L. (1996) The C-terminal region of human angiogenin has a dual role in enzymatic activity, *Proc. Natl. Acad. Sci. U.S.A. 93*, 3243−3247.
54. Borkakoti, N., Moss, D. A., and Palmer, R. A. (1982) Ribonuclease A: least squares refinement of structure at 1.45 Å resolution, *Acta Crystallogr. B38*, 2210−2217.
55. Martin, P. D., Doscher, M. S., and Edwards, B. F. P. (1987) The refined crystal structure of a fully active semisynthetic ribonuclease at 1.8 Å resolution, *J. Biol. Chem. 262*, 15930−15938.
56. Rybak, S. M., and Vallee, B. L. (1988) Base cleavage specificity of angiogenin with *Saccharomyces cerevisiae* and *Escherichia coli* 5S RNAs, *Biochemistry 27*, 2288−2294.
57. Pople, J. A. (1956) Proton magnetic resonance of hydrocarbons, *J. Chem. Phys. 24*, 1111.
58. Leonidas, D. D., Shapiro, R., Irons, L. I., Russo, N., and Acharya, K. R. (1999) Toward rational design of ribonuclease inhibitors: High-resolution crystal structure of a ribonuclease A complex with a potent 3′,5′-pyrophosphate-linked dinucleotide inhibitor, *Biochemistry 38*, 10287−10297.
59. Wodak, S. Y., Liu, M. Y., and Wyckoff, H. W. (1977) The structure of cytidilyl(2′,5′)adenosine when bound to pancreatic ribonuclease S, *J. Mol. Biol. 116*, 855−875.
60. Toiron, C., Gonzalez, C., Bruix, M., and Rico, M. (1996) Three-dimensional structure of the complexes of ribonuclease A with 2′,5′-CpA and 3′,5′-d(CpA) in aqueous solution, as obtained by NMR and restrained molecular dynamics, *Protein Sci. 5*, 1633−1647.
61. . Zegers, I., Maes, D., Dao-Thi, M.-H., Poortmans, F., Palmer, R., and Wyns, L. (1994) The structures of RNase A complexed with 3′-CMP and d(CpA): Active site conformation and conserved water molecules, *Protein Sci. 31*, 2322−2339.
62. Mohan, G., Boix, E., Evans, H. R., Nikolovski, Z., Nogues, M. V., Cuchillo, C. M., and Acharya, K. R. (2002) The crystal structure of eosinophil cationic protein in complex with 2′,5′-ADP at 2.0 Å resolution reveals the details of the ribonucleolytic active site, *Biochemistry 41*, 12100−12106.

BI030066H